ORIGINAL RESEARCH

Deep rolling of fine blanking punch edges

Numerical and experimental investigation of a novel deep rolling tool for filleting of cylindrical punches

F. Klocke[1] · A. Shirobokov[1] · D. Trauth[1] · P. Mattfeld[1]

Abstract Fine blanking is an economical process to manufacture components with a high sheared edge quality. Fine blanking of high-strength steels leads to an increase of the wear of fine blanking punches and deteriorates the economical efficiency of this process. In preliminary work lateral surfaces of cylindrical punches made of different hardened steels industrially used for tool manufacturing were deep rolled. Under proper process parameters a reduction of surface roughness, a hardness increase as well as an induction of compressive residual stresses in the surface layer were achieved. Therefore, deep rolling has a potential to improve the wear resistance of fine blanking punches. In order to improve the quality of the sheared edge of a workpiece, fine blanking punches must have a round fillet on the cutting edge. Filleting through plastic deformation can improve the wear resistance of this most loaded region of the fine blanking punch. In order to perform the filleting of the cutting edge through plastic deformation and to induce strain hardening and compressive residual stresses into the edge region a novel profiled deep rolling tool is developed in this work. Furthermore, the technical feasibility of the edge deep rolling with regard to the processing of fine blanking punches is assessed for the first time. The approach is based on a numerical modeling and experimental investigation of edge deep rolling.

Introduction

Initial situation Fine blanking is a mass production process conventionally attributed to the area of sheet metal forming. Fine blanked workpieces distinguish themselves through a high accuracy and quality of sheared surfaces. Manufactured under proper conditions fine blanked workpieces can be directly assembled with other components without any additional post-treatment operations required. In fine blanking the punch is one of the most loaded tool components. Therefore, it is susceptible to the highest wear [1]. During the cutting phase of the process the punch is compressed in its axial direction because of the resistance of the sheet metal being cut. After the actual cutting process is finished, the sheet metal springs back resulting in normal contact stresses acting on the punch circumference. Due to friction between the punch and the sheared edge tensile stresses in the axial direction of the punch arise. This leads to an exposure of the punch surface layer to a cyclic load which promotes material fatigue [2]. In the context of energy efficiency, light weight design of mechanical components is often realized through the implementation of high-strength materials [3]. Apart from high strength, these materials have high elasticity modulus and therefore are characterized by a bigger spring back [4]. Both factors lead to a more intensive cyclic loading of fine blanking punches and promote the punch wear. In order to

✉ A. Shirobokov
A.Shirobokov@wzl.rwth-aachen.de

F. Klocke
F.Klocke@wzl.rwth-aachen.de

[1] Laboratory for Machine Tools and Production Engineering (WZL) of RWTH Aachen University, Steinbachstr. 19, 52074 Aachen, Germany

increase the abrasive wear resistance fine blanking punches are conventionally manufactured from steel hardened up to 60 HRC. Additionally wear protective coatings are used [5]. However, no actions are usually taken in the conventional industrial practice in order to mitigate the fatigue wear of fine blanking punches due to the cyclic loading.

Deep rolling (DR) is an incremental forming process for the mechanical surface treatment of technical components. The general process principle consists in pressing of a rolling body against the workpiece so that local plastic deformation of the surface layer occurs [6]. This results in a smoothing of surface asperities as well as in an induction of compressive residual stresses and strain hardening in the surface layer [7, 9]. These factors impede the micro-crack initiation and propagation in a material under cyclic loads improving the fatigue strength [8]. Therefore, DR is conventionally implemented for the finish surface processing of cyclically loaded components such as crank shafts or axles [10, 11].

Deep rolling is a promising technology for an enhancement of the tool life of dynamically loaded fine blanking punches. Experimental and numerical characterization of the lateral surface layer state of cylindrical workpieces made of different tool steels and deep rolled with conventional deep rolling tools has been already performed in preliminary work [12]. A substantial reduction of surface roughness, an increase of the hardness as well as an induction of compressive residual stresses into the workpiece were attained. Furthermore, a FE process model of deep rolling of cylindrical surfaces was developed and validated with regard to the maximum value of the induced compressive residual stresses.

Motivation The geometry of the cutting edge of fine blanking punches has a significant influence on the stress distribution in the punch as well as on the resulting quality of the sheared edge. In order to increase the burnished zone, the cutting edge of a fine blanking punch should be filleted [13]. Furthermore, filleting of the cutting edge leads to a reduction of the stress concentration on the cutting edge, which promotes the tool life of punches [14]. Fillets on the cutting edge are performed through polishing so that no strain hardening and residual stresses are induced into the workpiece. Cutting edge region is, however, exposed to a cyclic load which causes material fatigue and results in the ultimate punch failure. In order to mitigate this effect the cutting edge region can be deep rolled. Usage of conventional deep rolling tools with a spherical rolling element results in an undefined deformation of the cutting edge due to the unconstrained material flow. Alternatively, the fillet on the cutting edge can be produced through plastic deformation so
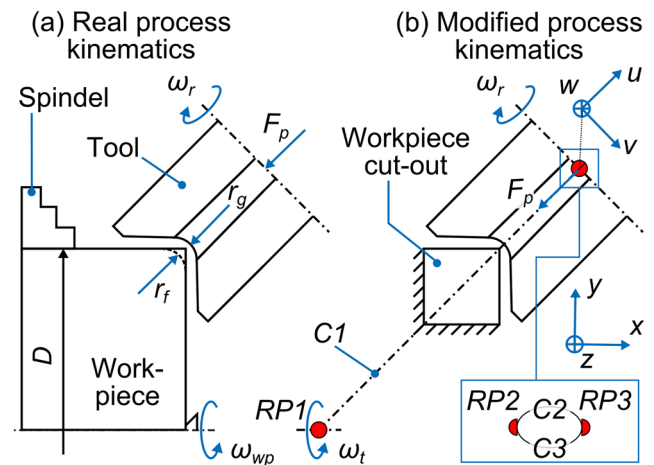
Fig. 1 Principal scheme of the edge deep rolling. Legend: ω_r - rotational velocity of the roller, F_p - Process force, D - workpiece diameter, r_r - roller radius, r_f - fillet radius, ω_{wp} - rotational velocity of the workpiece, ω_t - rotational velocity of the tool, $RP1(2, 3)$ - reference points, $C1(2, 3)$ - connectors, x, y, z - global coordinate axes, u, v, w - connector coordinate axes

that strain hardening and compressive residual stresses are induced into the cutting edge region. Currently no similar applications for the incremental filleting of the cylindrical edges by plastic deformation are known. Therefore, in the following this technical approach will be investigated for the first time.

Objective The aim of this research work is a numerical investigation and experimental validation of a novel edge deep rolling (EDR) process for the cutting edge filleting of cylindrical workpieces which will be performed for the first time. According to the intended application of EDR to the cutting edge filleting of fine blanking punches, processing of high-strength powder metallurgical high speed steel PMD23 (DIN 1.3395, AISI M3:2) is considered.

Approach In the scope of this work, a numerical process model of EDR with a profiled filleting tool is firstly developed. Then simulations to assess characteristic process parameters are performed. Based on the simulation results a prototype of a profiled edge deep rolling tool is manufactured. Thereafter experiments with a newly developed tool are performed and a validation of the simulation process model with regard to the achieved fillet geometry is realized. After that the surface layer state in the edge region is numerically assessed. Upon critical discussion of the results and possibility of the application of EDR to the processing of fine blanking punches further necessary research activities are formulated.

Process description of EDR

Principal scheme of the proposed EDR process is presented in Fig. 1. Subplot a depicts the real process kinematics and b the modified process kinematics as implemented in a numerical model of EDR (described in more detail in the following section). EDR is performed on a conventional lathe. The workpiece is clamped on the spindle of the lathe and rotates at rotational speed ω_{wp} around its axis. The filleting of the sharp cylindrical edge is performed by means of plastic deformation with a grooved roller. The roller has a symmetrical profile and is inclined by angle $\alpha = 45°$ to the workpiece. The profile radius of the grooved roller r_r corresponds to the desired fillet radius r_f of the workpiece. The rotational degree of freedom of the grooved roller against its cylindrical axis is unconstrained enabling rolling friction between the tool and the workpiece. Process force required for the deformation of the fillet F_p is applied to the grooved roller. As a result of material flow rounding of the edge as well as formation of the bulges on the face and lateral surfaces of the workpiece is expected. In order to study EDR in more detail and support the tool design a numerical process model of EDR on the basis of finite element method (FEM) is developed in the following section.

Numerical model development

FE simulation of deep rolling process has been in focus of scientific research for more than a decade [15, 16]. Common for most of the recent works is 3D modeling [17, 18] as well as the usage of the explicit time integration algorithm [19]. Generally, in order to numerically analyze the surface layer state after deep rolling a fine discretization of this region is required [20]. Furthermore, the overlap between single deep rolling lanes is proven to be a significant process parameter influencing the surface layer state [21]. In order to analyze this effect numerically 3D process models of deep rolling are employed. The usage of 3D modeling approach combined with the required fine discretization of the surface layer results in FE models having several hundred thousand elements. Furthermore, 3D FE process models demonstrate complex rapidly changing contact conditions so that the contact algorithms enforce the time increment reduction [22, 23]. The limitation of the time increment in conjunction with a big number of elements in a model would raise the computational costs significantly. Therefore, under these conditions explicit time integration algorithm is computationally more efficient than the implicit one [24]. From practical reasons further measures are also employed in order to further reduce the computational costs. These are modeling of a representative workpiece cut-out (see Figs. 1b and a) and usage of mass scaling technique.

The mass scaling may induce some artificial inertial effects into the FE process model that interfere with the simulation results. Therefore, in order to possibly avoid the inertial effects the deformable bodies (workpiece) have to be immovable in the model. This approach has been already successfully realized by Trauth et al. [21]. Based on these considerations development of an explicit dynamics 3D FE process model of EDR of a cylindrical cut-out element with Software *Abaqus 6.13* is described in the following paragraphs.

Workpiece and Tool The complete cylindrical workpiece with diameter $D = 50$ mm is reduced to a representative element having a shape of a sector being cut out from a tube with the axial length $l = 4$ mm, radial thickness $t = 4$ mm, and sector angle $\theta = 30°$ as shown in Fig. 2a. The premise for this simplification is that the effects of elastic bending of the workpiece due to the process force are insufficient and can be neglected. Based on the classical beam theory the elastic deflection of the workpiece as well as the maximum bending stresses were calculated. Corresponding to the real process the workpiece can be assumed as a cantilever beam with a length $l = 40$ mm (Fig. 6), diameter $D = 50$ mm and elasticity modulus $E = 230$ GPa loaded with the process force $F_p = 6.75$ kN. The beam deflection is $\delta_b = 1.4$ μm that results in a maximum bending stress of $\sigma_{b,max} = 0.016$ GPa. The elastic beam deflection and maximum bending stress are at least two orders of magnitude lower than the expected local material deformation in the edge region as well as the stresses in the forming zone. Therefore, it appears to be plausible to model only a representative cut-out of the workpiece without a significant loss of the modeling accuracy. The discretization of the deformable workpiece model was performed with linear continuum hexahedral elements with eight nodes. The workpiece model was partitioned in order to get a finely resolved mesh in the relevant edge region while keeping the element size in other regions more coarse. An additional partitioning of the finely resolved edge region had to be performed so that the element edges are aligned with the deformation load (Fig. 2b). By this means it is possible to avoid the mesh interlocking effect preventing the material deformation under arbitrary high process loads. Element size of 0.1mm and 0.5mm were used in the inside and outside of the edge region respectively. The total number of the workpiece elements is $n_{el,wp} = 45559$.

The only forming element of the EDR tool is a profiled roller. Therefore, only this component was reproduced in the FE model as shown in Fig. 2a. It is modeled as a discrete rigid cylindrical shell body with a profiled groove along its circumference and meshed with four nodes rectangular elements. Due to the symmetry of the groove the compete geometry of the tool in the FE model can
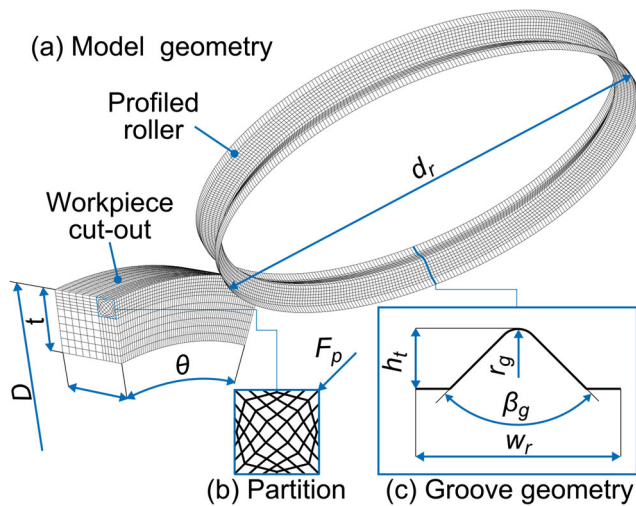
Fig. 2 Workpiece geometry (**a**) and discretization (**b**), profiled groove geometry (**c**). Legend: D - workpiece diameter, t - radial thickness, θ - sector angle, F_p - process force, d_r - roller diameter, β_g - groove angle, h_t - groove depth, r_g - groove fillet radius
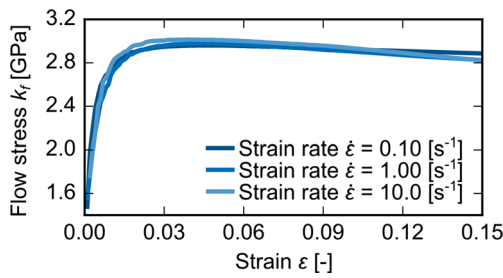
be described through the five parameters roller diameter d_r, groove angle β_g, groove depth h_t, and groove fillet radius r_g as shown in Fig. 2c. Element size of 0.1 mm was used to mesh the groove. The total number of roller elements is $n_{el,wp} = 64976$.

Additionally, it was checked if the reduced integration option of the elements of the chosen elements has an influence on the resulting stress and strain field distributions in the workpiece. Simulations with full integration elements C3D8 and S4 (workpiece and shell, respectively) and reduced integration elements C3D8R and S4R were performed. No significant differences between the resulting stress and strain fields after EDR were observed. Usage of full integration elements led however to a three times longer simulation duration. Therefore, reduced integration elements C3D8R and S4R were used in this model.

Kinematics In order to employ the mass scaling technique without induction of negative inertial effects the deformable workpiece should be immovable. This is realized by means of an encastre and symmetry boundary conditions applied to the workpiece as shown in Fig. 1b. Workpiece immobility requires an adaptation of the real process kinematic so that the relative motion between the tool and the workpiece can be reproduced in the FE model. This can be done by means of the substitution of the workpiece rotation ω_{wp} with the roller rotation ω_t about the workpiece axis with the same value of the absolute rotational velocity but oppositely directed. Realization of such kinematics in *Abaqus* can be made by means of connector elements which couple

or constrain translational and rotational degrees of freedom of the connected nodes. Generally, three connectors are to be defined in the model as shown in Fig. 1b. The first connector $C1$ should be defined between the reference point (RP) lying of the workpiece axis $RP1$ and another reference point $RP2$ on the roller axis. The purpose of this connector is to transfer the rotational motion of the $RP1$ to the $RP2$. Connector element $C1$ has only one translational degree of freedom along axis U of the local connector coordinate system. U direction is unconstrained in order to enable the tool movement along this direction due to process force F_p. Spatially $RP2$ coincides with the reference point of the tool $RP3$. In order to translate the rotation of $RP1$ to the tool, reference points $RP2$ and $RP3$ have to be connected. This can be done through the definition of two connections between them. One of them is a multi-point constraint of type pin $C2$. By these means translational degrees of freedom of the $RP3$ can be eliminated from the model reducing the total number of degrees of freedom [25]. By these means the $RP3$ and therefore the complete tool follow the spatial movement of the $RP2$ controlled by rotation of $RP1$. The second connection between $RP2$ and $RP3$ is required in order to ensure that the $RP3$ has only one rotational degree of freedom around the v axis (see Fig. 1b). This can be achieved by means of a connector element $C3$ between $RP2$ and $RP3$ suppressing rotational degrees of freedom of $RP3$ about axes u and w of the local connector coordinate system. Process kinematics realized according to the described approach is equivalent to that of the real EDR in terms of relative motion between the tool and the workpiece. It is designed to mitigate the artificial effects of mass scaling. Analogously to [21] a mass scaling factor $m = 250$ [-] was set in the model. In an industrial EDR process the workpiece performs several revolutions while being in contact with the tool. Due to the fact that the sample workpiece is immovable, multiple instances of the EDR tool are defined in the model to account for the number of rolling laps n_l. In order to reduce the total simulation duration with multiple tools two of them can be simultaneously in contact with the workpiece. Simultaneous tool motions are defined so that the distance between any two tools being in contact with the workpiece is a half of the tangential workpiece dimension θ_{wp}. This is realized through the usage of different amplitudes assigned to the velocity constraints of the tools.

Contact General contact is used as the contact algorithm. The tangential behavior is modeled with the penalty method. Constant friction coefficient according to Coulomb $\mu = 0.1$ [-] is set [20]. Normal contact behavior is defined with a hard contact property, prohibiting the penetration of the tool nodes into the workpiece.

Fig. 3 Experimentally determined flow curves of the workpiece material

Table 1 FE process model parameters: rolling velocity

Velocity	Laps	Force	Roller geometry			
ω_{wp} [r/min]	n_l [−]	F_p [kN]	D_r [mm]	β_g [°]	h_g [mm]	r_g [mm]
80						
400	3	1	50	91	1	0.3
800						

Material The workpiece material is a high alloyed powder metallurgical high speed steel PMD23 (DIN: 1.3395, AISI: M3:2) vacuum hardened to 60 HRC. This material demonstrates a high wear resistance and is industrially used for challenging blanking applications. The elasticity modulus was set to be $E = 230$ GPa according to the material specification. Two compressive tests at three strain rates $\dot{\varphi} = [0.1, 1, 10]$ s^{-1} each were performed at the Institute of Metal Forming (IBF) of RWTH Aachen University in order to characterize the plastic material behavior. The flow curves are plotted in Fig. 3. Hereby, obtained flow curves as well as the validation of the material behavior in FE software *Abaqus 6.13* was performed in preliminary work [12].

Investigation of EDR

In the scope of this work the developed FE model is firstly implemented prior to the experiments to get a first estimation of the process characteristics and interactions of the process factors with the resulting fillet geometry. The obtained insights were considered in the design phase of a prototype EDR tool. Upon the manufacturing of the tool and conducting of some experiments the FE model was adjusted according to the real tool shape and validated with regard to the resulting fillet geometry. Thereafter the validated model is used to analyze the surface layers state in the edge region after EDR.

Numerical pre-investigation of EDR

Before manufacturing of the prototype the influence of rolling velocity ω_{wp}, number of rolling laps n_l and rolling force F_p on the final shape of the fillet were analyzed by means of the developed FE process model of EDR. In order to do so an initial set of FE process model parameters was defined and successively adapted according to the obtained results. In the following paragraphs the model parameters as well as the results of the numerical pre-investigation of EDR are presented.

Rolling velocity Due to the strain rate dependent material behavior [12] the rolling velocity has a potential influence on the process result. In order to asses this effect three simulations with different rotational velocities ω_{wp} were performed. FE process model parameters are shown in Table 1.

The determination of the fillet radius was performed by reading out of the nodal coordinates of elements along the assessment path located at tangential position $\theta = 20°$ as shown in Fig. 4a. Determination of the fillet radius was realized through least-square fitting of an analytical circle to the nodal coordinate data. A *Python* script with fitting algorithm *leastsq* from *SciPy* library was implemented for this purpose.

No influence of the rolling velocity ω_{wp} on the fillet radius r_{wp} were observed (see Table 2). Models with higher rotational velocities have shorter processing times to be simulated. With the time increment being almost independent from the rotational velocity a considerable reduction of the total simulation duration in models with higher velocities is attained. Therefore, as no significant differences between the fillet geometries were observed rotational velocity $\omega_{wp} = 800$ rpm was used for the further simulations.

Number of rolling laps Another aspect to be considered in EDR process is the dependency of the edge deformation on number of rolling laps. In order to investigate this dependency a FE model with ten EDR tools, which corresponds
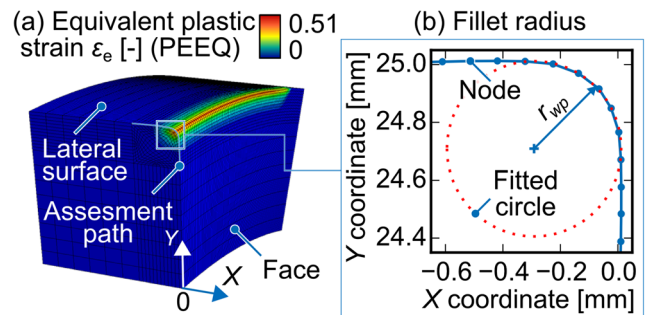
Fig. 4 Assessment path (**a**) and determination of the fillet radius (**b**). Legend r_{wp} - fillet radius

Table 2 Fillet radius: rolling velocity

| | Rotational velocity ω_{wp}[rpm] | | |
	80	400	800
Fillet radius r_{wp}[mm]	0.299	0.300	0.298

Table 4 Fillet radius: number of laps

| | Number of laps n_l[−] | | | | |
	1	3	5	8	10
Fillet radius r_{wp}[mm]	0.277	0.294	0.298	0.298	0.300

to ten revolutions of the workpiece in an industrial process, was defined. The model parameters are presented in Table 3.

The geometry of the workpiece was analyzed after the first, third, fifth, eighth, and tenth passage of the tool (i.e. workpiece revolution). The determination of the fillet radius was performed in the same way and at the same position as explained in Fig 4. The calculated radii are listed in Table 4. As can be observed there is no significant difference between the fillet radii after three laps. The relative deviation of the fillet radius after three laps to that after ten laps is $\delta = 2$ %. Therefore, due to the minor difference between the results three laps were used in the following simulations.

Rolling force For the reasons of the EDR tool design it is also necessary to get an estimation of the rolling force F_p required to perform the intended filleting operation. In order to obtain this data a series of simulations with different process forces F_p were performed. The model parameters are presented in Table 5.

As can be observed from Fig. 5 there is a direct correlation between the process force F_p and the resulting fillet radius r_g up to the threshold value $F_p = 3.5$ kN. The calculated fillet radii presented in Table 6. A further increase of the process force above does not seemingly influence the fillet geometry. An explanation for this behavior is the increasing contact area between the tool and the workpiece. At the beginning of the EDR process the contact area between the workpiece and the tool is the smallest so that high contact stresses initiate local material flow in the edge region. With an ongoing plastic deformation the contact area increases leading to a reduction of the local stresses in the edge region. This can lead to a discontinuation of the plastic deformation until reaching the form closure between the workpiece and the tool as it is the case for $F_p = 1$ kN and $F_p = 2$ kN. If the form closure between the workpiece and the tool is reached the local plastic deformation

is constrained by the tool. Therefore, a much larger region of the workpiece is exposed to the process force so that the resulting stresses are not sufficient to maintain further plastic deformation.
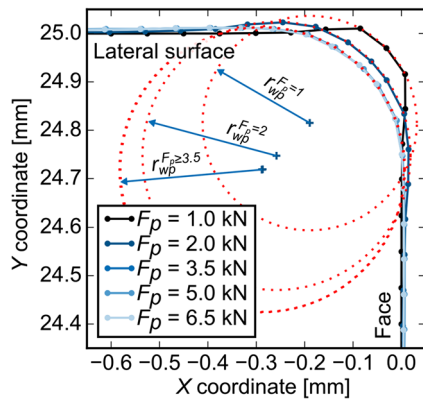
Drawing a preliminary conclusion to the numerical pre-investigation of the EDR it can be stated that this process appears to be robust against the variation of the process parameters rolling velocity, number of rolling laps, and process force. With regard to the possible industrial application of EDR it can be considered as an advantage since the required efforts to control the process are low.

Experimental investigation of EDR

Based on the numerical pre-investigation a prototype EDR tool was manufactured by Ecoroll AG Werkzeugtechnik Germany. Principal components of the tool as well as the measured groove geometry are shown in Fig. 6. The tool has a profiled roller placed in a fork. As far as the positioning of the tool with regard to the workpiece is performed manually the roller is mounted in the fork with a play of about 1 mm in axial direction. By this means it is intended to compensate for the inaccuracy of the manual EDR tool positioning. The fork attached to a shaft of a hydraulic cylinder that is used in a hydrostatic deep rolling tool HG19 from Ecoroll. Under applied hydraulic pressure the fork with the profiled roll is displaced until it comes into contact with a workpiece, and a hydrostatic pressure in the cylinder is build up generating the process force F_p. The fluid pressure is provided by an external hydraulic unit HGP from Ecoroll. Maximum process force is limited to $F_p = 9$ kN. Due to manufacturing tolerances the geometry of the roller slightly deviates from that used in the numerical pre-investigation.

Table 3 FE process model parameters: number of laps

| Velocity | Laps | Force | Roller geometry | | | |
ω_{wp} [rpm]	n_l [−]	F_p [kN]	D_r [mm]	β_g [°]	h_g [mm]	r_g [mm]
800	10	5	50	91	1	0.3

Table 5 FE process model parameters: number of laps

| Velocity | Laps | Force | Roller geometry | | | |
ω_{wp} [rpm]	n_l [−]	F_p [kN]	D_r [mm]	β_g [°]	h_g [mm]	r_g [mm]
800	3	1 2 3.5 5 6.5	50	91	1	0.3

Fig. 5 Influence of the process force F_p on the fillet radius r_{wp}

In order to experimentally prove the technical feasibility of EDR, a filleting of a ground cylindrical workpiece with a diameter $D = 50$mm made of powder metallurgical high speed steel PMD23 (DIN: 1.3395, AISI: M3:2) vacuum hardened to 60 HRC was performed. The experiment was conducted on a conventional lathe. The EDR tool was clamped in the tool holder at inclination angle $\alpha = 45°$ to the longitudinal axis of the workpiece. The parameter of the experiment are summarized in Table 7.

The resulting profile of the workpiece was measured with a profilometer and its contour was saved as a set of x and y coordinates. The *Python* script for the determination of the fillet radius was enhanced to perform a coordinate transformation of the measured profile so that its orientation corresponds to the numerically determined values. The fitting routine for the determination of the fillet radius remained unchanged. The experimentally achieved fillet profile is shown in Fig. 8.

Validation of the EDR FE process model

In order to asses the accuracy of the developed FE process model of EDR a simulation with the experimental parameters given in Table 7 was performed. The resulting fillet geometry is shown in Fig. 7. As in the previous cases the same fitting algorithm for the determination of the fillet radius was used for the experimental and numerical profiles. The relative difference between the fillet radii from the experiment $r_{wp,exp} = 0.285$ mm and simulation $r_{wp,sim} = 0.294$ mm is $\delta(r_{wp}) = 3$ %. Due to incompressibility of the metal simulative and experimental profiles demonstrate

Table 6 Fillet radius: number of laps

|	Process force F_p[kN]				
	1.0	2.0	3.5	5.0	6.5
Fillet radius r_{wp}[mm]	0.221	0.277	0.294	0.294	0.294
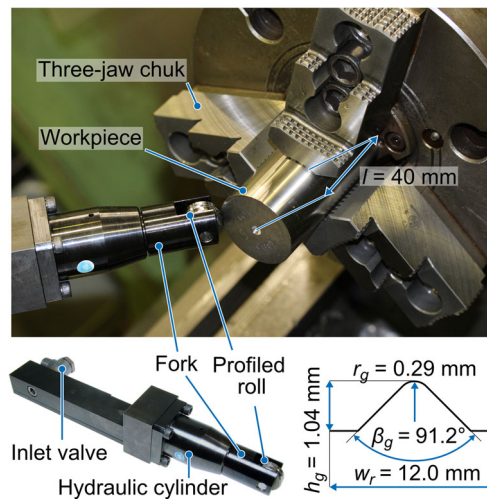
Fig. 6 EDR tool and the measured groove geometry

formation of bulges on lateral and face surfaces in the edge region. This leads to an increase of the maximum workpiece diameter ($\Delta(D_{exp}) = 0.016$ mm, $\Delta(D_{sim}) = 0.021$ mm) as well as the maximum length ($\Delta(l_{exp}) = 0.017$ mm, $\Delta(l_{sim}) = 0.005$ mm). The relative differences are $\delta(D) = 31$ % and $\delta(l) = 70$% respectively. Different bulging in the experiment and simulation can be explained by manual positioning of the EDR tool with regard to the workpiece as well as by the axial mobility of the roller. In the simulation model the roller is positioned symmetrically against the workpiece. Although the roller is mounted with a play in the fork to compensate possible positioning inaccuracies, the position of the tool relative to the workpiece in the experiment can deviate from that one in the FE model. This may lead to the observed quantitative differences between the maximum workpiece diameter and length.

Surface layer state after EDR

Due to the curved geometry of the edge zone and its small dimensions experimental characterization of the surface layer state is complicated and will be performed numerically. The developed and validated EDR FE process model enables the analysis of the stress and strain distributions after the EDR process. As can be seen from Fig. 8a there is an equivalent plastic strain localized in the edge region. The

Table 7 Experimental process parameters

| Velocity	Laps	Force	Roller geometry			
ω_{wp}	n_l	F_p	D_r	β_g	h_g	r_g
[rpm]	[−]	[kN]	[mm]	[°]	[mm]	[mm]
80	10	6.75	25	91.2	1.04	0.29
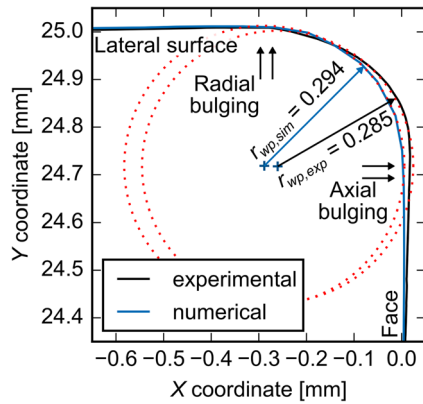
Fig. 7 Experimentally and numerically determined fillet profiles. Legend: $r_{wp,exp}$ - experimentally determined fillet radius, $r_{wp,sim}$ - simulative determined fillet radius

maximum equivalent plastic strain is achieved on the edge of the workpiece. Distribution of residual stresses in tangential and axial directions of the workpiece are presented in Fig. 8b and c respectively. As it can be observed, EDR induces a complex distribution of the residual stresses in the edge region. The highest tangential compressive stresses are shifted to the face of the workpiece. The highest values of the axial compressive stresses are on the lateral surface. It should be noted that there are tensile stresses in axial and tangential directions in the bulge area on the lateral surface. The tangential tensile stresses in the bulge region appear to be higher than axial tensile stresses. Distribution of the hydrostatic pressure is shown in Fig. 8d. Apart from the bulge region on the lateral surface positive hydrostatic pressure, indicating compressive hydrostatic stress, is induced in the workpiece.

Discussion of the results

Edge filleting of a cylindrical workpiece made of powder metallurgical high speed steel PMD23 (DIN: 1.3395, AISI: M3:2) vacuum hardened to 60 HRC by means of EDR is shown to be technically feasible. The plastic equivalent strain in the edge region indicates the strain hardening in the edge region. This increases the abrasive wear resistance as well as inhibiting fatigue crack initiation and propagation. Analysis of the residual stress state after EDR indicates a complex distribution of compressive and tensile residual stresses in the edge region. Except for the bulge region on the lateral surface compressive tangential and axial residual stresses as well as positive hydrostatic pressures are achieved through EDR in the edge region. This impedes the fatigue crack initiation and propagation. However, it can be clearly seen that there are moderate tensile residual stresses in axial and tangential directions as well as negative hydrostatic pressure in the bulge region on the lateral surface. This region is exposed to the axial tensile stresses during workpiece strip-off from the punch. Therefore, the tensile residual stresses in axial direction as well as negative hydrostatic pressure may promote the fatigue crack initiation and impair the fatigue strength of the punch. Furthermore, the diameter of a fine blanking punch determines the dimension of the workpiece and is tightly tolerated. For instance, a conventional fine blanking punch used in a real industrial process has a diameter $d_p = 50_{-0.01}$ mm. The diameter increase $\Delta(D)$ due to the bulging calculated in section "Validation of the EDR FE process model" leads to the violation of the diameter tolerance field. Therefore, an additional processing step after EDR has to be performed to restore
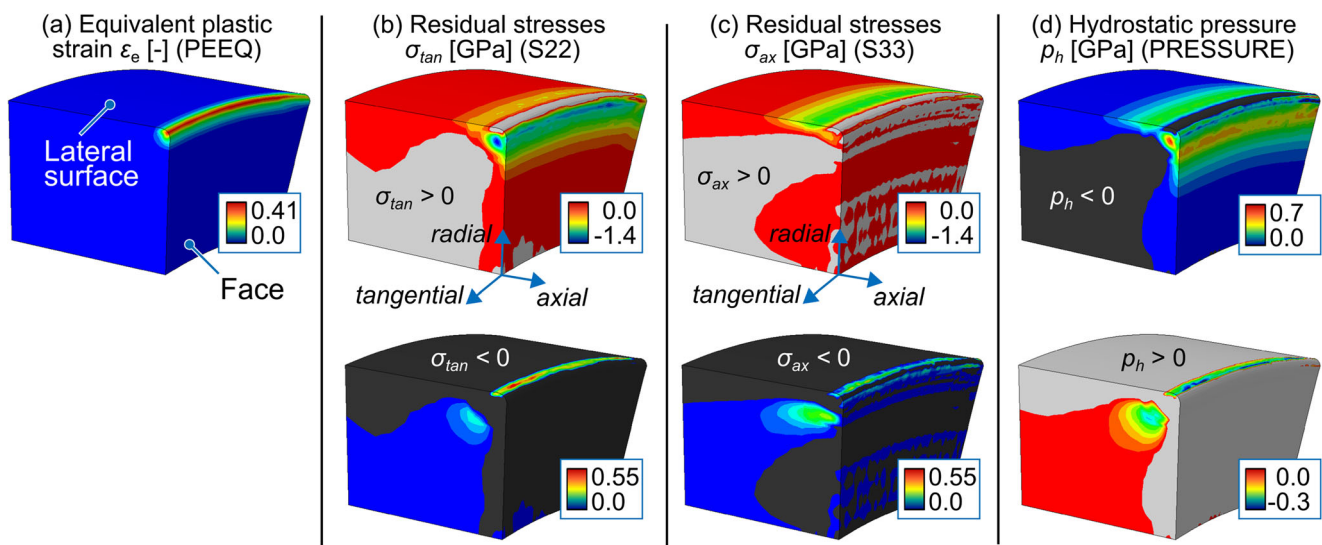
Fig. 8 Surface layer state after EDR. Legend: ϵ_e - equivalent plastic strain, σ_{tan} -residual stress in axial direction, σ_{ax} - residual stress in axial direction, p_h - hydrostatic pressure

the diameter dimension. Conventional deep rolling of the lateral surface can be used to simultaneously smoothen the bulge and restore the diameter dimension as well as to induce compressive residual stresses into the bulge region on the lateral surface. However, in order to do so appropriate process parameters will be defined in future work.

Conclusion and outlook

In the scope of this work a numerical investigation of EDR tool was performed. Based on this a EDR tool prototype was developed and manufactured. Thereafter, a technical feasibility of EDR for the edge filleting of a cylindrical workpiece made of powder metallurgical high speed steel PMD23 (DIN: 1.3395, AISI: M3:2), which is industrially used for highly loaded fine blanking punches, was proven. Based on the experiment the developed EDR FE process model was validated through the comparison of experimentally and numerically determined fillet radii. The FE model was used to analyze the surface layer state after EDR. With regard to the processing of fine blanking punches a critical area with tensile residual stresses as well as negative hydrostatic pressure in the bulge region on the lateral surface was identified. Furthermore, it was established that the bulging on the lateral surface leads to the violation of the dimensional tolerance on the punch diameter. Therefore, smoothing of the bulge on the lateral surface and induction of compressive residual stresses into this region is required in order to implement EDR for the filleting of fine blanking punches. A conventional deep rolling process of the lateral surface was proposed to achieve both aims.

In future work, numerical and experimental investigations of the EDR followed by a conventional deep rolling of the lateral surface will be performed. Based on the gained knowledge of the appropriate process parameters fine blanking punches for an industrial application will be deep rolled. Thereupon, a wear analysis of deep rolled fine blanking punches under industrial conditions will be performed. By these means it will be possible to quantify the influence of deep rolling on the tool life.

References

1. Luo SY (1999) Effect of the geometry and the surface treatment of punching tools on the tool life and wear conditions in the piercing of thick steel plate. J Mater Proc Tech 88:122–133. doi:10.1016/S0924-0136(98)00375-6

2. Sergejev F, Peetsalu P, Sivitski A, Saarna M, Adoberga E (2011) Surface fatigue and wear of PVD coated punches during fine blanking operation. Eng Fail Anal 18:1689–1697. doi:10.1016/j.engfailanal.2011.02.011

3. Sonsino CM (2007) Light-weight design chances using high-strength steels. Mat-wiss u Werkstofftech 38:9–22. doi:10.1002/mawe.200600090

4. Klocke F (2009) Manufacturing processes 4, forming. Springer, Berlin

5. Klocke F, Sweeney K, Raedt HW (2001) Improved tool design for fine blanking through the application of numerical modeling techniques. J Mater Proc Tech 115:70–75. doi:10.1016/S0924-0136(01)00771-3

6. Schulze V, Schwing JK (2006) Modern mechanical surface treatment. States, stability, effects. Wiley-VCH, Weinheim

7. Altenberger I (2005) Deep rolling-the past, the present and the future. In: Schulze V, Niku-Lari A (eds) Proceedings of 9th International Conference on Shot Peening ICSP-9, Paris, France

8. Niku-Lari A (1987) Advances in surface treatments. Pergamon Press, Oxford

9. Meyer D, Kruse D, Bobe A, Goch G, Brinksmeier E (2010) Nondestructive characterization of the surface integrity of cold surface hardened components. Prod Eng Res Devel 5:443–449. doi:10.1007/s11740-010-0228-3

10. Galzy F, Michaud H, Sprauel JM (2005) Approach of residual stress generated by deep rolling application to the reinforcement of the fatigue resistance of crankshafts. Mater Sci Forum 490-491:384–389. doi:10.4028/www.scientific.net/MSF.490-491.384

11. Abrão AM, Denkena B, Breidenstein B, Mörke T (2014) Surface and subsurface alterations induced by deep rolling of hardened AISI 1060 steel. Prod Eng Res Devel 8:551–558. doi:10.1007/s11740-014-0539-x

12. Klocke F, Shirobokov A, Mattfeld P, Feuerhack A (2014) Festwalzen von Feinschneidstempeln (in german) 10:660–665. wt-online

13. Hoffmann H (2012). Handbuch Umformen (in german) Hanser, Mnchen

14. Picas I, Hernndez R, Casellas D, Valls I (2010) Strategies to increase the tool performance in punching operations of UHSS. In: Proceedings of IDDRG 2010 Graz, Austria, pp 325–334

15. Röttger K (2003) Walzen hartgedrehter Oberflächen (in german). RWTH Aachen University, Dissertation

16. Mader S (2006) Festwalzen von Fan- und Verdichterschaufeln (in german). RWTH Aachen University, Dissertation

17. Manouchehrifar A, Alasvand K (2009) Finite element simulation of deep rolling and evaluate the influence of parameters on residual stress. In: Tsuomu K (ed) Recent Researches in Applied Mechanics. WSEAS Press, Athens, pp 121–127

18. Bäcker V, Klocke F, et al. (2010) Analysis of the deep rolling process on turbine blades using the FEM/BEM-coupling. IOP Conf Ser: Mater Sci Eng 10:012134. doi:10.1088/1757-899X/10/1/012134

19. Balland P, Tabourot L, Degre F, Moreau V (2013) An investigation of the mechanics of roller burnishing through finite element simulation and experiments. Int J Mach Tools Manuf 65:29–36. doi:10.1016/j.ijmachtools.2012.09.002

20. Perenda J, Trajkovski J (2015) Residual stresses after deep rolling of a torsion bar made from high strength steel. J Mater Proc Tech 218:89–98. doi:10.1016/j.jmatprotec.2014.11.042

21. Trauth D, Klocke F, Mattfeld P, Klink A (2013) Time-efficient prediction of the surface layer state after deep rolling using similarity mechanics approach. Procedia CIRP 9:29–34. doi:10.1016/j.procir.2013.06.163

22. Jung DW, Yang DY (1998) Step-wise combined implicitexplicit finite-element simulation of autobody stamping processes. J Mater Proc Tech 83:245–260. doi:10.1016/S0924-0136(98)00059-4

23. Noels L, Stainier L, Ponthot JP (2004) Combined implicit/explicit time-integration algorithms for the numerical simulation of sheet metal forming. J Comput Appl Math 168:331–339. doi:10.1016/j.cam.2003.12.004

24. Achmus C, Jung U, Kaiser B, Wohlfahrt H (1997) FEM-simulation des festwalzens von kurbelwellen (in german). Konstruktion 10:31–34

25. Systemes Dassault (2014) Abaqus Analysis User's Guide: Prescribed Conditions, Constraints & Interaltions